Bulletin of Mathematical Biology (2008) 70: 800–819
DOI 10.1007/s11538-007-9280-3

ORIGINAL ARTICLE

Two-Fluid Model of Biofilm Disinfection

N.G. Cogan

Department of Mathematics, Florida State University, 208 Love Building, Tallahassee, FL 32306, USA

Received: 27 October 2006 / Accepted: 19 September 2007 / Published online: 11 December 2007

Abstract We consider a dynamic model of biofilm disinfection in two dimensions. The biofilm is treated as a viscous fluid immersed in a fluid of less viscosity. The bulk fluid moves due to an imposed external parabolic flow. The motion of the fluid is coupled to the biofilm inducing motion of the biofilm. Both the biofilm and the bulk fluid are dominated by viscous forces, hence the Reynolds number is negligible and the appropriate equations are Stokes equations.

The governing partial differential equations are recast as boundary integral equations using a version of the Lorenz reciprocal relationship. This allows for robust treatment of the simplified fluid/biofilm motion. The transport of nutrients and antimicrobials, which depends directly on the velocities of the fluid and biofilm, is also included. Disinfection of the bacteria is considered under the assumption that the biofilm growth is overwhelmed by disinfection.

Keywords Biofilm · Two-fluid · Boundary integral method · Regularized stokeslets

1. Introduction

Because of the many health, environmental and industrial processes that are impacted by bacteria biofilms, understanding the failure of antimicrobial treatments is of paramount importance. Currently, there are several hypotheses concerning tolerance mechanisms including phenotypic, environmental and structural mechanisms (Davies, 2003; Lewis, 2001; Prakash et al., 2003; Lappin-Scott and Costerton, 1995; Desai et al., 1998; Keren et al., 2004). Because it is likely that all of the mechanisms play some role in conferring tolerance, mathematical models have been introduced to investigate these mechanisms (Balaban et al., 2005; Cogan et al., 2005; Cogan, 2005; Grobe et al., 2002; Sanderson and Stewart, 1997; Dodds et al., 2000).

In this investigation, we expand a previous continuum model of biofilm disinfection (Cogan et al., 2005) to include the coupled motion of the biofilm and the external fluid. In part, this is an important step in the development of a continuum model of disinfection

E-mail address: cogan@math.fsu.edu.
Supported by NSF award DMS-0612467.

that includes the material properties of the biofilm. However, we also find that the motion of the biofilm plays a role in the effectiveness of continuous dosing. This effect depends on the relative viscosities of the fluid/biofilm materials as demonstrated by simulations comparing the survival curves for varying biofilm viscosities. We also demonstrate the dependance of the disinfection efficiency on the initial biofilm/fluid interface geometry with simulations comparing several geometries.

The manuscript is organized as follows: The first section gives an overview of the model and numerical implementation. This has been described previously in more detail (Cogan, 2007), so the description will be relatively brief. We then describe the numerical simulations and comparisons. We conclude with a summary and discussion of the results.

2. Model description

2.1. Overview

The fundamental simplification that we make in this investigation concerns the material properties of the biofilm. It is well known that biofilm exhibit viscoelastic properties; however, the dominant behavior depends on the time-scale of interest. For disinfection, this time scale is on the order of hours while the relaxation time for biofilms has been estimated on the order of minutes (Shaw et al., 2005). Thus, the elastic forces will decay quickly compared to the time scale of the simulations allowing us to approximate the behavior of the biofilm as viscous, rather than viscoelastic. We treat the biofilm as a viscous fluid whose viscosity is much larger than that of the external bulk fluid. The length scale is set by a typical thickness of a biofilm which is on the order of 500 microns; the velocity scale depends on the experimental procedure. We are focusing our attention on low flow systems (Sanderson and Stewart, 1997) and using typical values for the velocities in these experiments and the viscosity of water as the reference viscosity. We find that the Reynolds number, which compares the inertial scales to the viscous scales, is much less than one. This indicates that the inertial terms are negligible and we will treat both the biofilm and the bulk fluid as viscous fluids governed by Stokes equations.

We also treat the problem in two dimensions rather than three. This simplification may alter the results presented to some extent as there are differences between flows in two and three dimensions. Currently, we have developed numerical methods that are applicable in higher spatial dimensions, although they have only been implemented for two dimensions. It is not clear how much variation there will be and although we believe that the qualitative results will translate, we plan to investigate the behavior in three dimensions later. Previous investigations compare mass transfer estimates in two and three dimensions and find that the results are comparable (Eberl et al., 2000).

Our model includes the coupled motion of the biofilm and the bulk fluid as well as the diffusion/advection of various constituents. The motion of the biofilm plays a role in the transport of the constituents as there is additional transport due to advection within the biofilm. To determine the various model components for each time-step, we determine the fluid and biofilm velocities as described below. Once the fluid and biofilm velocities are determined, we compute the advection, diffusion and reaction of the chemical substances. Since the chemical constituents equilibrate rapidly, the chemical concentrations are assumed to be at quasi-steady-state. The diffusion coefficient of all diffusing substances is

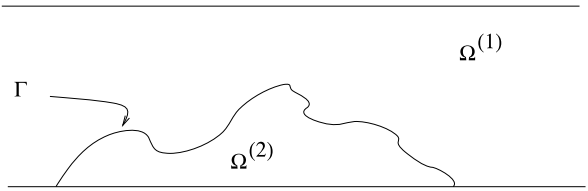

Fig. 1 Schematic of the domain, Ω. The region is separated into two sub-regions, $\Omega^{(1)}$, the bulk fluid region, and $\Omega^{(2)}$, the biofilm region, by an interface Γ.

reduced within the biofilm (Stewart, 1996). The reduction factor is not common for all chemicals, but is thought to be due to reduced permeability through physical and chemical interactions with the EPS. Because the biofilm/fluid interface is not sharp in general, the diffusion coefficient varies smoothly from the external fluid to the internal biofilm. We smooth the diffusion coefficient with a fixed transition region between the value in the bulk fluid and that in the biofilm (Cogan et al., 2005). The transition region is calculated independent of the discretization. This is also important for the numerical treatment of the constituent (e.g., nutrient) equations since diffusion equations with discontinuous coefficients require more sophisticated numerical methods (Leveque and Li, 1994). Finally, the bacterial concentration is determined by solving a conservation equation that includes disinfection and advection of the bacteria. Each of these equations and the numerical methods for approximating the solutions are described below.

2.2. Governing equations

2.2.1. Bulk fluid and biofilm motion

In our simulations, we are neglecting the growth of the biofilm, therefore, both fluids are incompressible. This assumption is discussed in detail below. The fluids occupy a region Ω, which is a channel for this manuscript and are separated by a surface, Γ. We denote the two subregions as $\Omega^{(1)}$ and $\Omega^{(2)}$ for the bulk fluid and biofilm regions, respectively (see Fig. 1).

The dynamics of both the bulk fluid and the biofilm are governed by the incompressible Stokes equations

$$\nabla \cdot \sigma^{(*)} = 0, \tag{1}$$

$$\nabla \cdot \mathbf{U}^{(*)} = 0, \tag{2}$$

where $* = 1, 2$ denotes variables in the bulk and biofilm regions, respectively. Stokes equations describe conservation of momentum and mass with stress tensor $\sigma^* = P^*\mathbf{I} + \mu^*(\nabla\mathbf{U}^* + \nabla\mathbf{U}^{*\mathbf{T}})$ containing the hydrostatic pressures, P^*, and the viscous stresses proportional to the deformation gradient tensor. The constant of proportionality, μ^*, is the viscosity.

There are several methods for treating the two fluid problem including immersed interface (Layton, 2007; Mayo, 1985; Leveque and Li, 1997), immersed boundary (Mittal and Iaccarino, 2005) and the boundary integral method (Cogan, 2007; Cortez et al., 2005; Hou et al., 2001; Pozrikidis, 2001). We choose to transform the equations governing the

materials in each subdomain, $\Omega^{(1)}$ and $\Omega^{(2)}$ (i.e., bulk fluid and biofilm), into a single integral equation whose solution is the velocity at each point in the domain. This method is referred to as the boundary integral method (BIM) and is described in more detail below. We refer to the velocity of the system obtained using BIM as $\mathbf{U}$.

This model is applicable to fully developed biofilms rather than biofilms during the initial stages of growth. We expect that thin or developing biofilms will require substantially different treatment. This also raises a question about the interfaces with which we initialize our simulations. Because we see different dynamic behavior for various viscosities, the geometry of the biofilm as it develops presumably depends on various parameters and constituents. We do not account for the differences in the development but rather show how different initial geometries alter the dynamics of the system. At this time, separating the scales of biofilm development seems a reasonable method of analyzing the effects of varying geometries and material parameters although in the future a developing biofilm model will be derived and analyzed.

2.2.2. Constituents

Disinfection of the bacteria within a biofilm depends on many factors. There have been numerous experimental (Davies, 2003; Grobe et al., 2002; Prakash et al., 2003; Hentzer et al., 2003; Sufya et al., 2003; Lewis, 2001) and mathematical (Roberts and Stewart, 2004; Dodds et al., 2000; Sanderson and Stewart, 1997; Cogan et al., 2005) investigations of various biofilm resistance mechanisms. There is no consensus on the dominant mechanisms; however, because typical antimicrobial agents and antibiotics are most effective at killing respiring bacteria (Lappin-Scott and Costerton, 1995), spatially dependent nutrient consumption leads to regions of lowered biocide effectiveness. This effect is referred to as physiological protection.

In several recent papers (Cogan et al., 2005; Grobe et al., 2002; Roberts and Stewart, 2004), models of physiological protection are considered. Because the action of typical antibiotics and biocides depends on the growth rate, these models require the disinfection rate to depend directly on the nutrient availability. In Cogan et al. (2005), this is done by assuming that the disinfection rate is proportional to the bacterial growth rate, and hence depends implicitly on the nutrient concentration. This has the effect of delaying the action of an antimicrobial within the biofilm since the bacteria near the fluid interface consume the nutrient leading to nutrient-depleted regions. These regions will not be susceptible to antimicrobial agents since they have zero growth rate. One of the observations that can be made about this tolerance mechanism is that it is transient. Because the bacteria near the interface are also more susceptible to disinfection, they are killed quickly. This allows the nutrient to penetrate further into the biofilm reducing the nutrient depleted zones inducing susceptibility. Throughout we are assuming that there is one growth-limiting substrate although this could be extended to other situations.

Because of the link between local nutrient availability and disinfection, accurate, realistic models of the dynamics of nutrient and antimicrobial concentrations must be considered. Since the diffusion of chemical constituents is fast compared to the time-scale of biofilm motion, we describe the concentrations of nutrient, $S(\mathbf{x}, t)$, and antimicrobial agent, $A(\mathbf{x}, t)$, by reaction/diffusion/advection equations at quasi-steady-state,

$$\mathbf{U}(\mathbf{x}, t) \cdot \nabla S(\mathbf{x}, t) = \nabla \cdot \big(D_s \nabla S(\mathbf{x}, t)\big) - \mu_s \frac{S}{K_s + S} B(\mathbf{x}, t), \tag{3}$$

$$\mathbf{U}(\mathbf{x}, t) \cdot \nabla A(\mathbf{x}, t) = \nabla \cdot \big(D_a \nabla A(\mathbf{x}, t)\big) + R(A, B, S), \tag{4}$$

where B denotes the bacterial concentration. The diffusion coefficients of nutrient and antimicrobial agent, $D_s(\mathbf{x})$ and $D_a(\mathbf{x})$, are assumed to be smaller in the biofilm region than in the bulk flow region with reduction factors are denoted r_s and r_a, respectively. The consumption of nutrient by the bacteria is modeled by Monod kinetics, where μ_s and K_s denote the maximum specific consumption rate and Monod coefficient, respectively. The maximum consumption rate is related to the maximum growth rate through the yield rate. In particular, the ratio of the consumption rate and the growth rate indicates the amount of substrate required to produce a unit mass of biomass, i.e., the yield. Both nutrient and antimicrobial are fed into the system at the upstream end of the channel, so the Dirichlet boundary conditions are applied at $x = 0$. Standard outflow conditions are applied at the effluent end of the channel. The walls of the channel are not permeable to the constituents, so we apply no-flux boundary conditions there.

The reaction term in Eq. (4) depends on the antimicrobial agent since some agents are highly reactive with components of the biofilm. For this investigation, we will assume that there is no reaction ($R \equiv 0$) which implies that the antimicrobial agent equilibrates to the source concentration, thus eliminating the need to compute the solution to Eq. (4). Our results are applicable to treatment with antibiotics such as ciprofloxacin that has been shown to fully penetrate biofilms without inactivation (Anderl et al., 2000) or biocides such as chlorosulfamate that have been shown to have very limited inactivation (Stewart et al., 2001).

2.2.3. Bacteria

The bacterial population at a point in space is changed by the advection of the biofilm as well as by disinfection. We assume that the disinfection of bacteria is proportional to the product of nutrient consumption and the bacterial concentration. Thus, bacteria that are exposed to higher nutrient levels are more susceptible to the antimicrobial agent. Combining these, we find the equation governing the bacterial concentration is

$$\frac{\partial B}{\partial t} + \nabla \cdot (\mathbf{U}B) = -\alpha \frac{S}{K_s + S} B(\mathbf{x}, t), \tag{5}$$

where B is zero outside the biofilm region. The coefficient α reflects the particular biocide. In this investigation, we are not comparing the results for differing biocides. Moreover, we have assumed that the antimicrobial has equilibrated, thus α is constant. Other forms of the disinfection rate have been investigated where more sophisticated disinfection models are developed (Cogan et al., 2005; Sanderson and Stewart, 1997; Roberts and Stewart, 2004; Cogan, 2005). We impose no-flux boundary conditions on the channel walls and Dirichlet conditions ($B = 0$) at the influent end. At the effluent end, we impose outflow conditions allowing the bacteria to be transported out of the domain; however, we have ensured that our computational domain is sufficiently large and that the cluster does not reach the end of the domain.

In the absence of disinfection, the bacteria within the biofilm would reproduce and continue to produce EPS; however we assume a constant application of disinfectant and that the disinfection rate is related to the consumption rate. If the concentration of the disinfectant is sufficiently high, disinfection will dominate growth. In particular, for our model of disinfection, the disinfection rate is highest precisely where the growth rate would be highest. Thus, one can consider the right-hand side of Eq. (5) as the cumulative effect of growth and disinfection. Thus, there is no net production of bacteria but rather a decline.

2.3. Numerical implementation

2.3.1. Velocities

The boundary integral method for treating fluid problems in various parameter regimes has been extensively studied in the past several decades. This method relies on the existence of a Green's function for the PDE operators. The immediate practicality of this method is apparent for fluids that can be treated as inviscid or as Stokes fluids (Pozrikidis, 2001; Hou et al., 2001). In either of these cases, Greens functions for various domains are readily obtained.

The main idea behind BIM is to use a version of the Lorenz reciprocal relation (Lorenz, 1907) to recast the governing PDEs as boundary integral equations. In general, the reciprocal identity allows one to obtain information about a given flow, $\mathbf{U}$, using information about another known flow, $\mathbf{U}'$. Because the flow field for a viscous fluid with a singular force can be calculated directly (Cortez, 2001), we use this as the comparison flow. Once the reciprocal relation is derived, the governing equations can be recast as integral equations whose domain is the boundary between the fluids.

We relate the unknown velocity $\mathbf{U}^*$ to the flow induced by a singular force with intensity $\mathbf{f}$ at a point $\mathbf{x}_0$. Thus, $\mathbf{U}'$ is a fundamental solution to incompressible Stokes equations,

$$\nabla \cdot \sigma' = \mathbf{f}\delta(\mathbf{x} - \mathbf{x}_0), \tag{6}$$

$$\nabla \cdot \mathbf{U}' = 0, \tag{7}$$

where $\sigma' = -P'\mathbf{I} + \mu(\nabla\mathbf{U}' + \nabla\mathbf{U}'^{\mathbf{T}})$. Again, P' is the hydrostatic pressure and μ is the viscosity. This is a convenient flow to use since the analytic solution can be computed easily using Fourier transforms (Pozrikidis, 1992). In two spatial dimensions, the solution is

$$\begin{aligned}\mathbf{U}'(\mathbf{x}) &= -\frac{\mathbf{f}}{4\pi\mu}\ln(r) + \mathbf{f}\cdot(\mathbf{x}-\mathbf{x}_0)\frac{(\mathbf{x}-\mathbf{x}_0)}{4\pi\mu r^2} \\ &= -\frac{\mathbf{f}}{4\pi\mu}\mathbf{G},\end{aligned} \tag{8}$$

where $r = \|\mathbf{x} - \mathbf{x}_0\|$ and $\mathbf{G}$ is the two-dimensional Stokeslet. The corresponding pressure and stress tensor are

$$P' = \frac{\mathbf{f}\cdot(\mathbf{x}-\mathbf{x}_0)}{2\pi r^2},$$

$$\sigma' = -\frac{\mathbf{f}}{4\pi\mu}\mathbf{T}.$$

The reciprocal relation for the bulk flow is determined by relating solutions to Eqs. (1) and (2) to (6), (7). By direct calculation, we find that

$$\nabla\cdot(\mathbf{U}\sigma') - \nabla\cdot(\mathbf{U}'\sigma) = \delta(\mathbf{x}-\mathbf{x}_0)\mathbf{U}, \tag{9}$$

which is the classical reciprocal relation.

Integrating the reciprocal relation, with various placements of the singular force (i.e., with $\mathbf{x}_0$ within $\Omega^{(1)}$ and $\Omega^{(2)}$), we recast Eqs. (1) and (2), with $* = 1$ as an integral

equation whose domain is the interface Γ. The integral equation relates the bulk fluid velocity to the traction jump across the interface, denoted $\Delta\sigma = (\sigma^{(1)} - \sigma^{(2)})$, and the velocity (see (Pozrikidis, 1992, Chapter 5)). The jth component of the bulk fluid velocity at $\mathbf{x}_0$ is

$$\mathbf{U}_j^{(1)}(\mathbf{x}_0) = -\frac{1}{4\pi\mu^{(1)}}\int_\Gamma \Delta\sigma_{ik}\eta_k(\mathbf{x})\mathbf{G}_{ij}(\mathbf{x},\mathbf{x}_0)\,dl(\mathbf{x}) + \frac{1-\lambda}{4\pi}\int_\Gamma \mathbf{U}_i(\mathbf{x})\mathbf{T}_{ijk}(\mathbf{x},\mathbf{x}_0)\eta_k(\mathbf{x})\,dl(\mathbf{x}), \tag{10}$$

where $\lambda = \frac{\mu^{(2)}}{\mu^{(1)}}$ and η is the outward unit normal. Here $j = 1, 2$ corresponds to the horizontal and vertical directions, respectively. In a similar manner, we obtain an integral equation for the motion of the biofilm,

$$\mathbf{U}_j^{(2)}(\mathbf{x}_0) = -\frac{1}{4\pi\mu^{(2)}}\int_\Gamma \Delta\sigma_{ik}\eta_k(\mathbf{x})\mathbf{G}_{ij}(\mathbf{x},\mathbf{x}_0)\,dl(\mathbf{x}) + \frac{1-\lambda}{4\pi\lambda}\int_\Gamma \mathbf{U}_i(\mathbf{x})\mathbf{T}_{ijk}(\mathbf{x},\mathbf{x}_0)\eta_k(\mathbf{x})\,dl(\mathbf{x}). \tag{11}$$

These two integral equations govern the coupled motion of the external bulk fluid and the internal biofilm. Because the flows must be continuous at the boundary, we can obtain the boundary velocity by taking limit of Eqs. (10) and (11) as $\mathbf{x}_0$ moves to the boundary. These limits both converge to

$$U_j(\mathbf{x}_0) = -\frac{1}{2\pi\mu^{(1)}(\lambda+1)}\int_\Gamma \Delta\sigma_{ik}\eta_k(\mathbf{x})\mathbf{G}_{ij}(\mathbf{x},\mathbf{x}_0)\,dl(\mathbf{x}) + \frac{\kappa}{2\pi}\int_\Gamma^{\mathcal{PV}} \mathbf{U}_i(\mathbf{x})\mathbf{T}_{ijk}(\mathbf{x},\mathbf{x}_0)\eta_k(\mathbf{x})\,dl(\mathbf{x}), \tag{12}$$

where $\kappa = \frac{1-\lambda}{1+\lambda}$. The latter integral is an improper integral that must be handled with care. There are many methods for evaluating this integral that depend on the dimension of Γ as well as the kernel of the integral. In this situation, the singularity is integrable and straightforward quadrature rules work well (Pozrikidis, 2001).

To close the system in a straightforward manner, we impose a constitutive relation relating the jump in traction, $\Delta\sigma_{ik}$ to mean curvature $\Delta\sigma = \gamma\eta\nabla\cdot\eta$ (see Pozrikidis, 1992). The magnitude of the surface tension is given by the constant of proportionality, γ.

Although Eq. (12) gives the velocity at the interface, the advection/diffusion of the chemical constituents requires the velocity throughout the domain. One could use Eqs. (10) and (11) to determine the velocity away from the interface; however, a more effective method has been developed in Cogan (2007). This method uses Eq. (12) to determine the velocity of the interface. This in turn, is used as data to determine forces that must be applied to the domain so that the material (fluid or biofilm) moves with the calculated velocities at the interface. These forces are then used to determine the velocities within the domain by exploiting the linearity of Stokes equations. More details can be found in Cogan (2007), Cogan et al. (2005). Essentially, this hybrid method uses BIM to determine the boundary motion and the method of regularized Stokeslets to determine the velocity away from the boundary.

We enforce no-flow conditions on the channel walls by imposing zero flow at discrete points on the walls. This inflates the number of points at which forces are applied on the fluid. Another advantage to this method is that inflow and outflow conditions do not need to be specified. These are determined by the superposition of the background flow and the singularity flows. In our simulations, the background flow is parabolic which is consistent with viscous flow in a channel.

To solve Eq. (12), we are confronted with a system of coupled integral equations which can be written as

$$\mathbf{W} = \mathbf{b} + \frac{\kappa}{2\pi} \int_{\Gamma} \mathbf{K}\mathbf{W}\, dl(\mathbf{x}), \tag{13}$$

where $\mathbf{W} = (\mathbf{U}_1^{(1)}, \mathbf{U}_2^{(1)})$. The vector $\mathbf{b}$ contains the Stokeslet and the tensor $\mathbf{K}$ contains the related stress tensor, both of which are known.

A straightforward method for solving the discretized integral equations is Nyström's method (Vetterling et al., 2002) which requires a quadrature rule:

$$\int_a^b y(s)\, ds = \sum_{j=1}^{n} \omega_j y(s_j),$$

where ω_j denotes the weights of the quadrature rule. For our simulations, we use Gauss–Legendre quadrature.

Both the vector $\mathbf{b}$ and the kernel of the integral equation have integrable singularities. This can make naive Nyström's method unstable. We choose to regularize these terms using the method of regularized Stokeslets. For this, we solve the regularized version of the singular Stokes' equation

$$\nabla \cdot \sigma = \mathbf{f}_0 \phi_\epsilon(\mathbf{x} - \mathbf{x}_0), \tag{14}$$

$$\nabla \cdot \mathbf{U} = 0, \tag{15}$$

where $\phi_\epsilon(\mathbf{x} - \mathbf{x}_0)$ denotes a cutoff or *blob* function. There are many choices for the regularization term ϕ_ϵ that yield regularized Stokeslet and stress (Cortez, 2001).

Once we have the regularized stresses, we discretize the initial interface into n control points. We then solve Eq. (13), with the vector $\mathbf{b}$ and the kernel $\mathbf{K}$ replaced with the regularized version.

Applying the quadrature rule to the regularized problem

$$\mathbf{W} = \mathbf{b}_\epsilon + \frac{\kappa}{2\pi} \int_{\Gamma} \mathbf{K}_\epsilon \mathbf{W}\, dl(\mathbf{x}), \tag{16}$$

yields a discrete system of the form

$$\mathbf{W}(\mathbf{x}_0) = \mathbf{b}(\mathbf{x}_0) + \frac{\kappa}{2\pi} \sum_{j=1}^{n} \mathbf{K}_\epsilon(\mathbf{x} - \mathbf{x}_0)\mathbf{W}(\mathbf{x})\omega_j. \tag{17}$$

Evaluating this at the n control points leads to

$$\mathbf{W}(\mathbf{x}_{0,i}) = \mathbf{b}\mathbf{x}_{0,i} + \frac{\kappa}{2\pi} \sum_{j=1}^{n} \mathbf{K}_\epsilon(\mathbf{x}_{0,i} - \mathbf{x}_j)\mathbf{W}(\mathbf{x}_{0,i})\omega_j. \tag{18}$$

This system can be inverted using any convenient iterative solver (i.e., gmres or conjugate gradient) since the kernels are symmetric and positive definite due to the symmetry of the regularized Stokeslet. Moreover, the kernel is positive definite since the Stokeslet has an integrable singularity at the interface, which has been smoothed by regularizing the Stokeslet. Once the velocities of the interface are calculated, we use techniques developed in Cortez (2001) to obtain the velocities away from the interface. The boundary points are then moved at their prescribed velocity, a new boundary is determined and the process is repeated.

2.3.2. Constituents

The steady-state nutrient concentration is determined numerically using ADI with second order-accurate upwinding to avoid excessive numerical diffusion. The diffusion coefficient varies between the biofilm region and the bulk fluid region. This is primarily due to the restriction imposed by the polymeric component of the biofilm. Rather than treat the diffusion coefficient as discontinuous, we smooth the values between D_{bulk} and D_{biofilm} the bulk and the biofilm region by a continuous approximation of the Heaviside function. This allows for standard treatment of the diffusion/advection equation as well as yielding an approximation that is independent of the discretization. This is also consistent with experimental observations that the density of the biofilm varies with depth. More details can be found in Cogan et al. (2005).

2.3.3. Bacterial concentration

We use a simple implementation of the method of lines with second order upwinding and Matlab's ode-suite to solve the discretized bacterial advection and disinfection equation. Thus, we discretize the spatial component of the bacterial concentration where the advection terms are given explicitly. This yields a system of ODEs which are solved with a fourth order Runge–Kutta algorithm.

3. Simulations

It is often advantageous for bacteria to form biofilms either to evade predation (i.e., human immune system) (Costerton, 2001) or to take advantage of alternative metabolic processes. In Klapper et al. (2002), the authors argue that the biofilms ability to react elastically to transient stresses and viscously to long term stresses allows the biofilm to stay in environmentally favorable environments while avoiding catastrophic material failures.

This investigation was motivated by the need to understand how biofilms protect the bacteria from disinfection. In particular, because the estimated viscosity of the biofilm is extremely high compared to that of the bulk fluid (Klapper et al., 2002), we would like to understand what effect the viscosity of the biofilm has on disinfection. Although there are many possible tolerance mechanisms, we only include physiological tolerance (i.e., nutrient dependent disinfection) and delayed penetration via a diffusional barrier. We then compared the disinfection curves for varying biofilm viscosities.

Since the biofilm moves with the fluid, one could argue that the motion of the biofilm should decrease the effectiveness of the disinfectant since the bacteria move away from the nutrient source. This tends to reduce the nutrient concentration available to the bacteria

Table 1 Parameters used in the simulations

Parameter	Symbol	Units	Value	Source
Maximum specific consumption rate	μ_s	h^{-1}	0.417	(Roberts and Stewart, 2004)
Yield coefficient	Y_b		0.8	(Roberts and Stewart, 2004)
Monod coefficient	K_s	$mg\,l^{-1}$	0.1	(Roberts and Stewart, 2004)
Nutrient influent concentration	C_s	$mg\,l^{-1}$	10	(Roberts and Stewart, 2004)
Nutrient diffusion coefficient	D_s	$m^2\,h^{-1}$	9.67×10^{-6}	(Roberts and Stewart, 2004)
Biofilm/bulk diffusivity reduction	r_*		0.9	(Sanderson and Stewart, 1997)
Length scale	L	m	10^{-2}	Assumed
Max. flow rate	$U_{\max}$	$m\,h^{-1}$	0–3.4	Assumed
Disinfection rate coefficient	α		0.4	Assumed
Biofilm viscosity	$\mu^{(2)}$	cP	1–5000 × water	Assumed

which in turn increases the physiological tolerance. Alternatively, one could argue that the dynamics of the biofilm interface could increase the effectiveness since the surface area is enlarged as the biofilm moves with the fluid allowing for easier penetration of nutrient and a subsequent decrease in physiological tolerance. In the absence of a compelling heuristic argument or experimental results, mathematical modeling and simulations are used to address the question. Parameters for the simulations are given in Table 1.

The range of biofilm viscosities is actually much lower than values estimated in the literature (Shaw et al., 2005). For the fluid regimes that we are studying and with the high viscosity of the biofilm, we find very little difference in disinfection results using a dynamic interface as compared to the fixed interface simulations in Cogan et al. (2005). This has several implications for modeling efforts. In particular, our results seem to support the idea that assuming a fixed interface may be a reasonable simplification for a range of flow regimes. This reduction substantially reduces the complexity of numerical methods and this result provides additional evidence to support this assumption. These results also show that the fixed domain treatment described in Cogan et al. (2005) is consistent with the dynamic model presented here as the biofilm viscosity increases. However, we also explore ranges of viscosity where the interface cannot be assumed stationary. This is done to help gain insight into the dependence of the advection/diffusion of the constituents and the disinfection on the simplest available material parameter.

3.1. Simulation 1: generic interface

In this set of simulations, we consider the disinfection of a generic biofilm cluster whose initial geometry is shown in Fig. 2. Survival curves were generated by simulating the effect of disinfection where we have assumed that the biocide has equilibrated to a constant concentration and the nutrient source is constant. The survival of the bacteria is given by $\log(\frac{\int B}{\int B_0})$, where B_0 is the initial concentration of bacteria. This gives the ratio of surviving bacteria as a function of time. We considered the effects of varying the viscosity of the biofilm over several orders of magnitude. In Fig. 3, we show the survival curves for various biofilm viscosities. As the viscosity increases, we see a decrease in the effectiveness of the disinfection. The survival curves converge to that of the fixed biofilm as the viscosity increases. It is apparent the viscosity plays a role in the disinfection efficiency. In Figs. 4–7, we show the domain and contours of the nutrient concentrations for varying

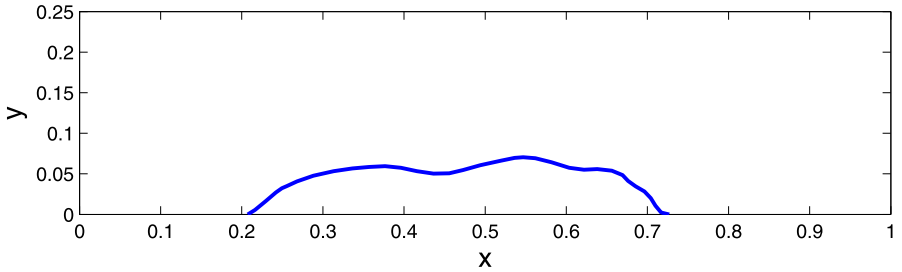

Fig. 2 Initial generic interface used in Simulation 1.

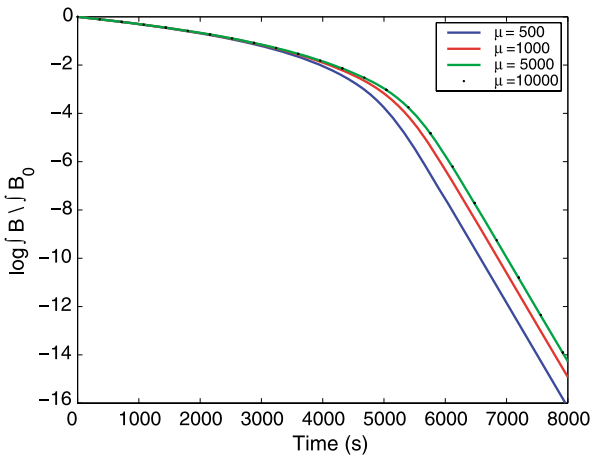

Fig. 3 Comparisons of the survival curves for varying viscosities. As the viscosity increases, we see a delay in the disinfection indicating that the less viscous biofilms are more susceptible to treatment than the higher viscosity biofilms. As the viscosity increases, the survival curves converge to that of the fixed biofilm domain as indicated by the overlap between the curves for $\mu^{(2)} = 5000$ and $\mu^{(2)} = 10000$. (Color figure online.)

viscosities. Evidently, the nutrient is better able to penetrate the biofilm with lower viscosity. This seems to support the hypothesis that the expansion of the surface area increases the susceptibility of the bacteria.

3.2. Simulation 2: time scale of disinfection

One motivation for the present investigation is to understand the effects of simplifying assumptions on the time-scale of disinfection and the transport of constituents into the biofilm. The simplest model to analyze neglects the fluid motion and treats the transport of nutrients and biocides into the biofilm as a diffusion dominated process. In an earlier investigation, we contrasted this with simulations which take the external flow into account but neglect the biofilm motion (Cogan et al., 2005). Here, we are able to include motion of both the external fluid and the biofilm. To quantify the difference, we considered methods to determine when the "knee" of the observed disinfection curves occur.

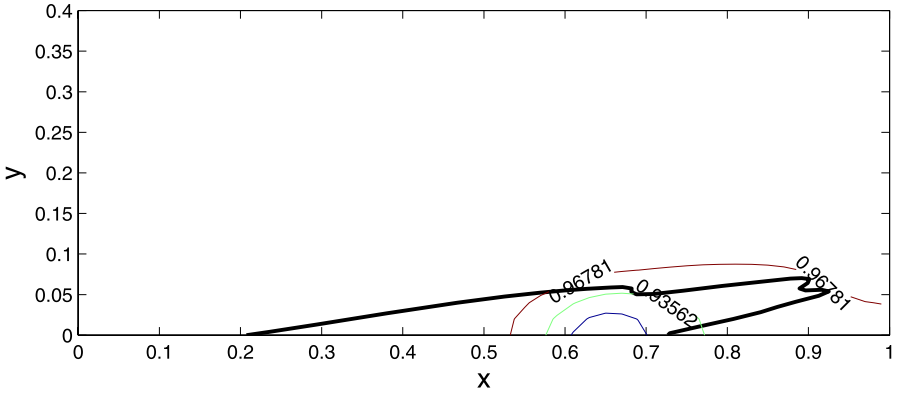

Fig. 4 This shows a snapshot of the biofilm with viscosity $\mu^{(2)} = 500$ at time $t = 96$ (min). The evolved interface is shown along with labeled contours of the nutrient levels. Here the nutrient has almost fully penetrated the biofilm, the bacteria are all susceptible at close to their maximum rate. (Color figure online.)

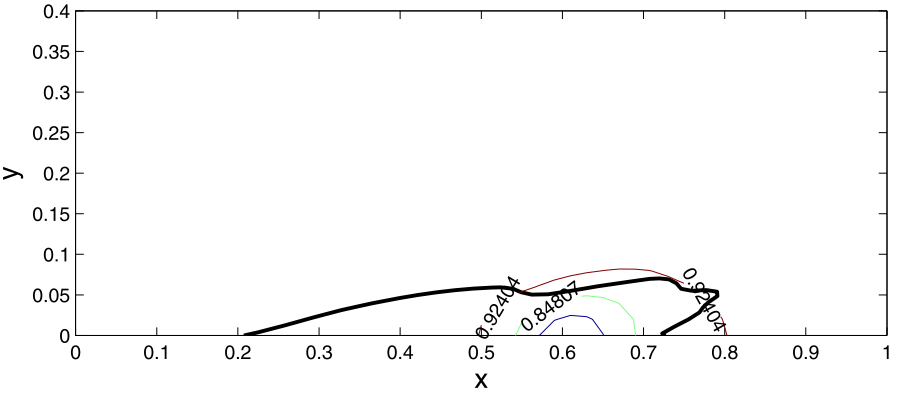

Fig. 5 This shows a snapshot of the biofilm with viscosity $\mu^{(2)} = 1000$ at time $t = 96$ (min). The evolved interface is shown along with labeled contours of the nutrient levels. The nutrient has not penetrated as far as the simulation with $\mu^{(2)} = 500$ indicating that there is some level of protection being offered to the bacteria as seen in the survival curves in Fig. 3. (Color figure online.)

The time at which the disinfection rate is maximal depends on the penetration time of the nutrient since the disinfectant rate depends on the nutrient availability and the biocide (which is constant in these simulations). To determine this time scale, we use the time course of nutrient concentration determined by the numerical simulations. We find the time at which the minimum values of the nutrient within the biofilm domain is .05 and .5 of the nutrient source concentration, $t_{.05}$ and $t_{.5,}$ respectively. In Fig. 8, we indicate these times on the survival curve for the generic interface and $\mu^{(2)} = 1{,}000$ indicating that these times are covering the "knee" of the curve. We also show the penetration time $t_{.5}$ as a function of viscosity in Fig. 9 for the generic interface.

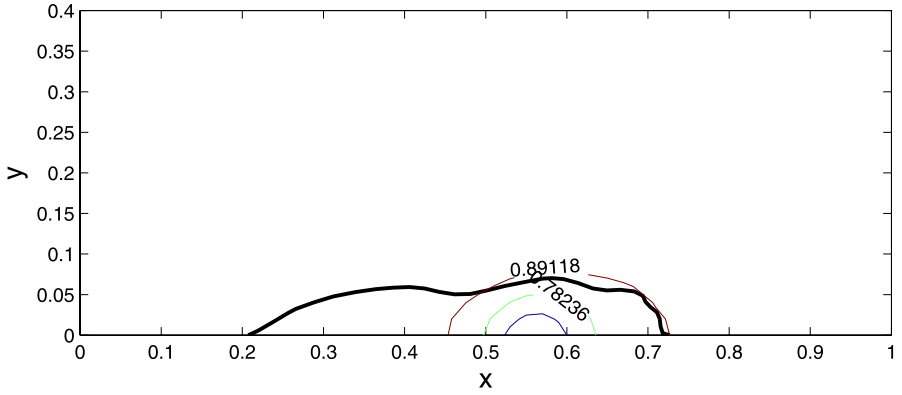

Fig. 6 This shows a snapshot of the biofilm with viscosity $\mu^{(2)} = 5000$ at time $t = 96$ (min). The evolved interface is shown along with labeled contours of the nutrient levels. Again, this is consistent with the results shown in Fig. 3. (Color figure online.)

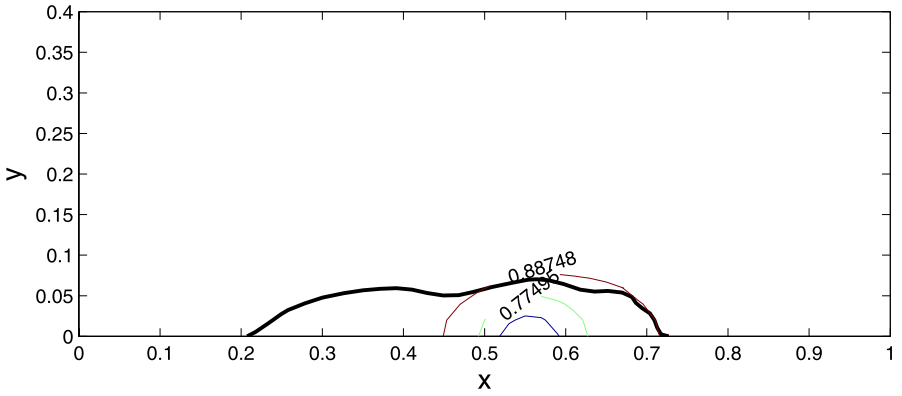

Fig. 7 This shows a snapshot of the stationary biofilm at time $t = 96$ (min). The interface is shown along with labeled contours of the nutrient levels. (Color figure online.)

Finally, we consider several other models of biofilm disinfection and compare the penetration times. In particular, we would like to determine the effects the motion of the biofilm region and the external flow have on the survival curves and penetration times. In Stewart (1996), the author calculates the penetration time for various antimicrobial agents (e.g., nonreactive, reactive, sorbing) for a flat slab biofilm with no external flow. Instead, the concentration of the biocide is constant at the interface. This can be upgraded to include a mass transfer boundary layer to incorporate the external flow in a qualitative manner.

We consider three simulations: The first is a numerical experiment that is similar to the analytic results in Stewart (1996) where the bulk fluid is well mixed and there is no external flow. The second incorporates explicit treatment of the external fluid with a fixed interface, and the final includes the motion of the biofilm and the external fluid. In each

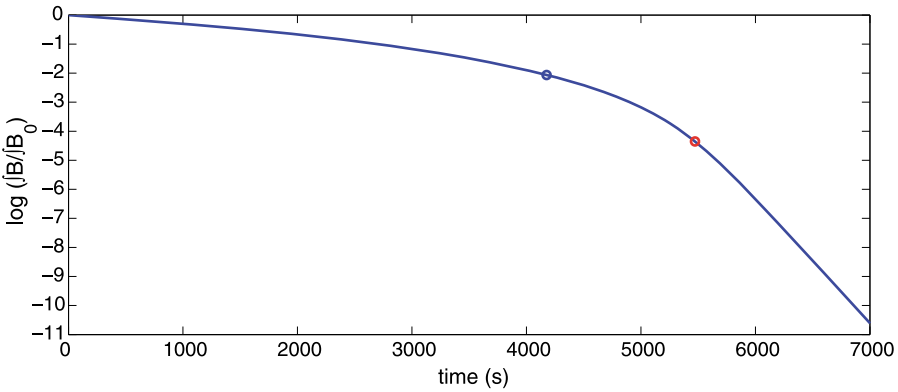

Fig. 8 Survival curves with the time at which the nutrient has penetrated so that the minimum value within the biofilm region is .05, indicated by the blue circle, and .5, indicated by the red circle. This indicates a measure of the dependence of the disinfection on the penetration of the nutrient. (Color figure online.)

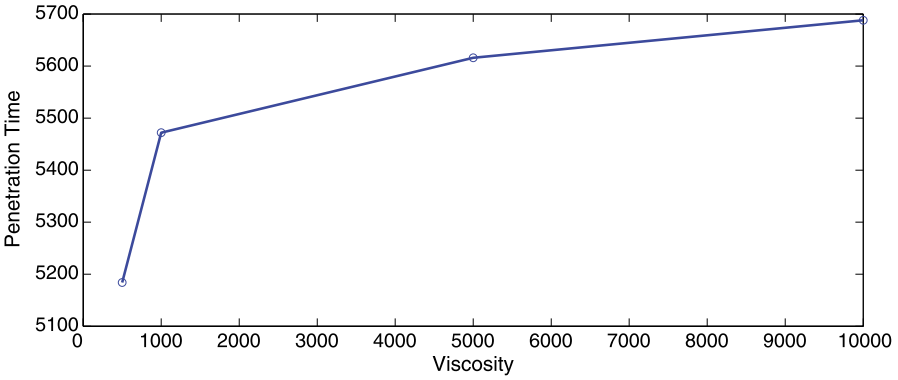

Fig. 9 A comparison of the time at which the minimum nutrient concentration is .5 within the generic biofilm domain for varying viscosities.

of these simulations, the initial interface is a hemisphere of radius .5. As in the rest of the manuscript, our disinfection model allows us to track the nutrient concentration in order to track the disinfection of the biofilm. For the first simulation, a boundary layer of the nutrient concentration is fixed at the interface and we consider diffusion of the nutrient into the biofilm. In the second simulation, we account for the motion of the external fluid while the biofilm region is fixed. In the third simulation, we allow for the biofilm to move as a viscous fluid with viscosity 500 times that of water. In Fig. 10, we show the survival curves as well as the times at which the nutrient has penetrated to .05 and .5% of the source concentration. We are well able to capture the "knee" of the survival curve. We also see that the pure diffusive case under-estimates the penetration times.

The times at which the minimum nutrient concentration is 0.5 are 2.4200, 2.1600 and 1.6600 hours for the fixed geometry with no flow, fixed geometry with flow and the moving domain, respectively. We chose to examine the case when the viscosity of the biofilm

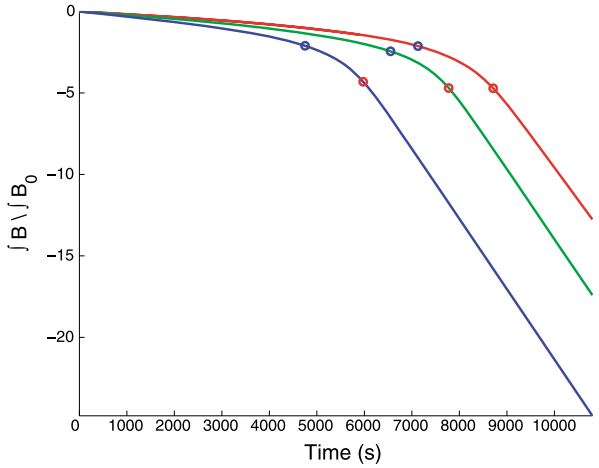

Fig. 10 Survival curves for three simulations with the time at which the nutrient has penetrated so that the minimum value within the biofilm region is .05, indicated by the blue circle, and .5, indicated by the red circle. The survival curves for no external or internal flow (red), no internal flow (green) and both external and internal flows (blue) are shown. (Color figure online.)

was only 500 times that of the bulk fluid to clearly demonstrate the difference between the fixed biofilm and the dynamic biofilm results. As the viscosity of the biofilm increases, the blue curve will collapse to the green curve.

3.3. Simulation 3: interface roughness

To further explore the relationship between the disinfection curves and the biofilm/fluid interface as the viscosity of the biofilm changes, we follow the method outlined in (Cogan et al., 2005). We develop three different domains with the same area but different biofilm/fluid interfaces. The interfaces are determined by a periodic function with three different periods. The three domains that are used are shown in Fig. 11. We the compare the survival curves for each of the three domains while varying the biofilm viscosity.

Previously, we have shown that for the stationary biofilm, the survival was decreased as the surface roughness increased (Cogan et al., 2005). This qualitative trend is true when the biofilm domain is nonstationary. We show the survival curves for three different viscosities in Fig. 12. In all cases, the domain with the rougher (i.e., shorter period) interface is more susceptible to disinfection. This effect is more pronounced as viscosity increases.

Differences in the arc length of the interfaces also relate to differences in the survival curves. In Fig. 13, we show the arc lengths as functions of time for each of the three domains and viscosities. The survival curves are correlated to the arc length since domains with larger arc lengths are more susceptible to disinfection. Examining this figure, we see that for $\mu^{(2)} = 500$ after 14,000 seconds, the arc length of the roughest initial interface is approximately five times that of the smoothest initial interface. At the same time, the survival differs by almost seven orders of magnitude. For $\mu^{(2)} = 1{,}000$, after 2,000 seconds, the arc length of the roughest initial interface is approximately three times that of the

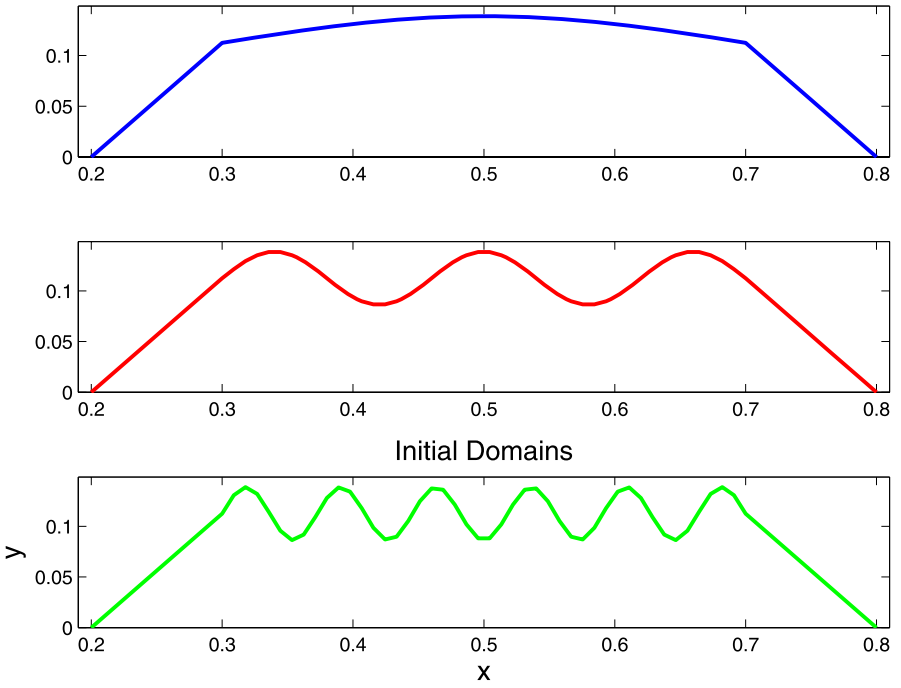

Fig. 11 This shows the three different initial domains used in simulation set 4. All domains have the same area, and since the bacterial concentration is uniformly distributed the same biomass. (Color figure online.)

smoothest initial interface. The survival curves at that time differ by approximately five orders of magnitude. For $\mu^{(2)} = 5{,}000$, the arc length of the roughest interface is approximately twice that of the smoothest after 25,000 seconds. The survival curves differ by less than two orders of magnitude. Thus, the relative difference in arc length corresponds to differences in the order of magnitude separation in survival.

These simulations are related to the studies outlined in Morgenroth et al. (2000), Eberl et al. (2000), where generic interfaces were developed. In those studies, changes in the mass transport into the biofilm for various random geometries was investigated. The external fluid dynamics was governed by the Navier–Stokes equations. In Eberl et al. (2000), the three dimensional case was studied and compared to the two-dimensional studies shown in Picioreanu et al. (2000). The results from these numerical studies was that the transport of mass into the biofilm via a diffusion limited process was enhanced by increased fluid flow and typically decreased with the surface roughness. Because the disinfection model we are assuming, relates the disinfection rate to the nutrient concentration; this seems to imply that for slowly flowing fluid systems mass transfer is actually enhanced by surface roughness. Thus, it seems that the fluid regime can alter the relationship between mass transfer and surface roughness.

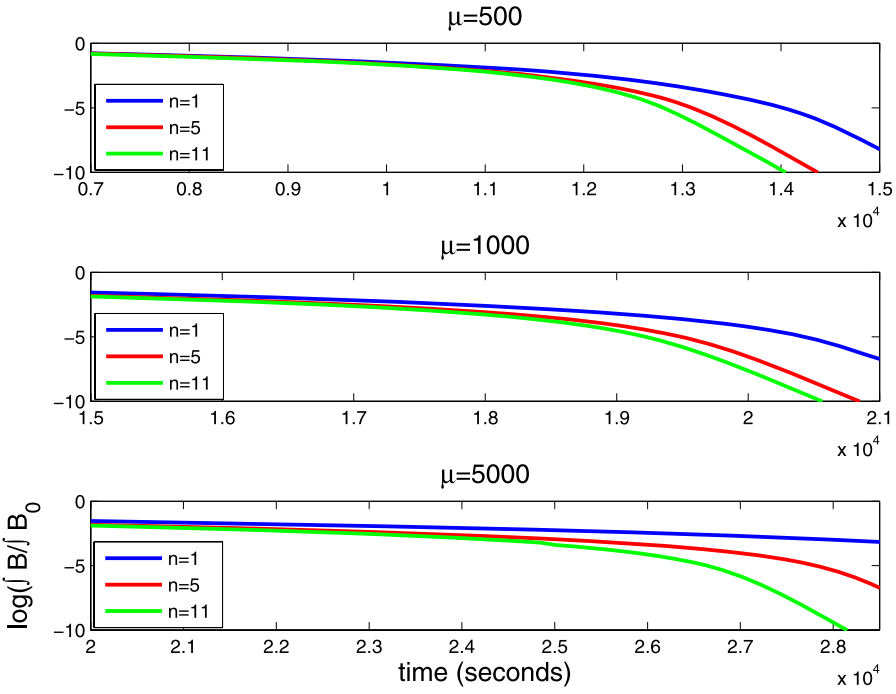

Fig. 12 This shows the survival curves for three different biofilm viscosities. The upper panel is for $\mu^{(2)} = 500$ while the biofilm viscosity was 1000 and 5000 the middle and lower panels, respectively. The effect of the initial surface roughness is more apparent as the viscosity increases. Note that the plots have been truncated to focus on the 'knee' of the survival curves. (Color figure online.)

4. Discussion

By allowing the biofilm domain to move in response to the fluid motion, we have found that disinfection is delayed as the biofilm viscosity increases. This suggests that if the viscosity of bacteria could be artificially decreased, say by heating the substratum, disinfection might be enhanced. Another method of altering the biofilm viscosity was investigated recently by Chen and Stewart (2002). Here the investigators noted that treating a biofilm with salts or chelating agents caused a large drop in the measured viscosity. Because of the observed differences in the survival curves for varying viscosity discussed above, we feel that this might be a viable method for increasing the effectiveness of treatment. It is interesting to note that a decrease in survival after dosing a biofilm with antibiotic and a chelator was demonstrated recently (Banin et al., 2006).

We have also considered how the nutrient penetration time sets the maximum disinfection rate. This time scale is contrasted with other simplified models. In particular, as the viscosity of the biofilm decreases, the penetration time decreases. This indicates that although diffusion within the biofilm can delay the penetration of chemicals, neglecting the external and internal flows has a measurable effect on the estimate of penetration times.

Although this investigation was motivated by incorporating the motion of the biofilm into a model of biofilm disinfection, we have applied this to a restricted class of applica-

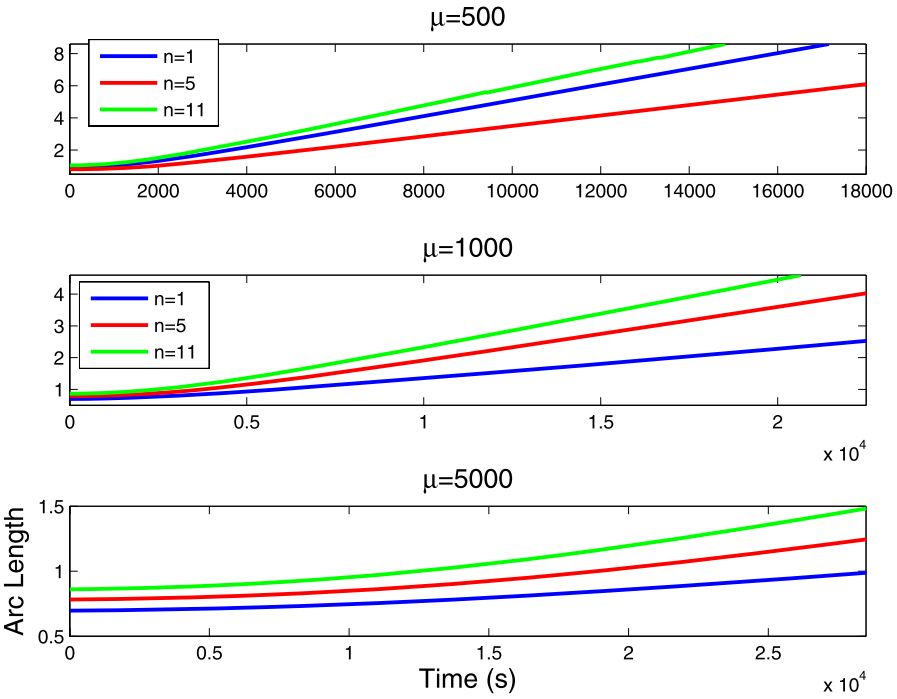

Fig. 13 We show the arc lengths as functions of time for each of the three domains (indicated by the legends) with varying viscosities. Domains with larger arc length are more susceptible to disinfection. The increase in arc length, which is more pronounced for lower viscosity also correlates with the increase in susceptibility. (Note that the axis are not the same for each figure.) (Color figure online.)

tions. For creeping flow at the rates used here, experimentally obtained biofilm viscosity implies that the biofilm domain does not move appreciably. We have seen that the survival curves converge to those obtained for a fixed biofilm region as the biofilm viscosity increases. In a sense, this observation serves as a validation of the model and implementation. Although the time-scales for the numerical simulations are short enough that the biofilm motion is negligible for experimental values of the viscosity, the biofilm motion is observed on a longer time scale. This motion plays a role in the development of biofilm structure in the absence of disinfectant which is an application that will be investigated in the future.

In conclusion, we have been able to show that the fixed biofilm reduction may be valid for disinfection models. This substantially reduces the complexity of the numerical methods that can be applied. We have also shown that the geometry and the material properties of the biofilm need to be accounted for to obtain accurate predictions. This also points to several important questions that have not yet been addressed. In particular, we have not considered the initial stages of biofilm growth. Because the geometry of the developing biofilm depends on the viscosity, it is not clear how varied the geometry will be. To address this, the growth of the biofilm must be included in the model.

We have also elucidated how the fluid regime affects the transport of various constituents. In particular, our results contrast those obtained in other numerical investigations (Eberl et al., 2000; Picioreanu et al., 2000). Thus, for systems with creeping flow, biofilm roughness may play an important role in disinfection.

Acknowledgements

This work was supported by NSF award DMS-0612467.

References

Anderl, J.N., Franklin, M.J., Stewart, P.S., 2000. Role of antibiotic penetration limitation in *klebsiella pneumoniae* biofilm resistance to ampicillin and ciprofloxacin. Antimicrob. Agents Chemother. 44, 1818–1824.

Balaban, N.Q., Merrin, J., Chait, R., Kowalik, L., Leibler, S., 2005. Bacterial persistence as a phenotypic switch. Science 305, 1622–1625.

Banin, E., Brady, K.M., Greenberg, E.P., 2006. Chelator-induced dispersal and killing of *Pseudomonas aeruginosa* cells in a biofilm. Appl. Environ. Microbiol. 72, 2064–2069.

Chen, X., Stewart, P., 2002. Role of electrostatic interactions in cohesion of bacterial biofilms. Appl. Microbiol. Biotechnol. 59, 718–720.

Cogan, N.G., 2005. Effects of persister formation on bacterial response to dosing. J. Theor. Biol. 88, 2525–2529.

Cogan, N.G., 2007. Hybrid numerical treatment of two-fluid problems with passive interfaces. Commun. Appl. Comput. Sci. 2(1).

Cogan, N.G., Cortez, R., Fauci, L.J., 2005. Modeling physiological resistence in bacterial biofilms. Bull. Math. Biol. 67, 831–853.

Cortez, R., 2001. The method of regularized stokeslets. SIAM J. Sci. Comput. 23, 1204–1225.

Cortez, R., Fauci, L., Medovikov, A., 2005. The method of regularized stokeslets in three dimensions: analysis, validation, and application to helical swimming. Phys. Fluids 17, 1–14.

Costerton, J., 2001. Cystic fibrosis pathogenesis and the role of biofilms in persistent infection. Trends Microbiol. 9, 50–52.

Davies, D., 2003. Understanding biofilm resistance to antibacterial agents. Nat. Rev. Drug Discov. 2, 114–122.

Desai, M., Buhler, T., Weller, P., Brown, M., 1998. Increasing resistance of planktonic and biofilm cultures of *Burkholderia cepeciax* to ciproflaxacin and ceftazidime during exponential growth. J. Antimicrob. Chemother. 42, 153–160.

Dodds, M.G., Grobe, K.J., Stewart, P.S., 2000. Modeling biofilm antimicrobial resistance. Biotechnol. Bioeng. 68, 456–465.

Eberl, H., Picioreanu, C., Heijnen, J., van Loosdrecht, M., 2000. A three-dimensional numerical study on the correlation of spatial structure, hydrodynamic conditions, and mass transfer and conversion in biofilms. Chem. Eng. Sci. 55, 6209–6222.

Grobe, K., Zahler, J., Stewart, P., 2002. Role of dose concentration in biocide efficacy against *Pseudomonas aeruginosa* biofilms. J. Ind. Microbiol. Biotechnol. 29, 10–15.

Hentzer, M., Wu, H., Andersen, J.B., Riedel, K., Rasmussen, T.B., Bagge, N., Kumar, N., nd Zhijun Song, M.A.S., Kristoffersen, P., Manefield, M., Costerton, J.W., Molin, S., Eberl, L., Steinberg, P., Kjelleberg, S., Hoiby, N., Givskov, M., 2003. Attenuation of *Pseudomonas aeruginosa* virulence by quorum sensing inhibitors. EMBO J. 22, 3803–3815.

Hou, T.Y., Lowengrub, J.S., Shelley, M.J., 2001. Boundary integral methods for multicomponent fluids and multiphase fluids. J. Comput. Phys. 169, 302–362.

Keren, I., Kaldalu, N., Spoering, A., Wang, Y., Lewis, K., 2004. Persister cells and tolerance to antimicrobials. FEMS Microbiol. Lett. 230, 13–18.

Klapper, I., Rupp, C., Cargo, R., Purvedorj, B., Stoodley, P., 2002. Viscoelastic fluid description of bacterial biofilm material properties. Biotechnol. Bioeng. 80, 289–296.

Lappin-Scott, H.M., Costerton, J.W. (Eds.), 1995. Microbial Biofilms. Cambridge University Press, Cambridge. Ch. Mechanisms of the Protection of Bacterial Biofilms from Antimicrobial Agents, pp. 118–130.

Layton, A.T., 2007. Modeling water transport across elastic boundaries using an explicit jump method. SIAM J. Sci. Comput. 28(6), 2189–2207.

Leveque, R.J., Li, Z., 1994. The immersed interface method for elliptic equations with discontinuous coefficients and singular sources. SIAM J. Numer. Anal. 31, 1019–1044.

Leveque, R.J., Li, Z., 1997. Immersed interface methods for Stokes flow with elastic boundaries or surface tension. SIAM J. Sci. Comput. 18, 709–735.

Lewis, K., 2001. Riddle of biofilm resistance. Antimicrob. Agents Chemother. 45, 999–1007.

Lorenz, H.A., 1907. Ein allgemeiner satz, die bewegung einer reibenden flussugkeit betreffend, nebst einigen anwendungen desselben. Abhand. Theor. Phys. 1, 23–42.

Mayo, A., 1985. Fast high order accurate solution of Laplace's equation on irregular regions. SIAM J. Sci. Comput. 6, 144–157.

Mittal, R., Iaccarino, G., 2005. Immersed boundary methods. Annu. Rev. Fluid Mech. 37, 239–261.

Morgenroth, E., Eberl, H., van Loosdrecht, M., 2000. Evaluating 3d and 1d mathematical models for mass transport in heterogenous biofilms. Water Sci. Technol. 41, 347–356.

Picioreanu, C., van Loosdrecht, M.C.M., Heijnen, J.J., 2000. A theoretical study on the effect of surface roughness on mass transport and transformation in biofilms. Biotechnol. Bioeng. 68, 355–369.

Pozrikidis, C., 1992. Boundary Integral and Singularity Methods for Linearized Viscous Flow. Cambridge University Press, Cambridge.

Pozrikidis, C., 2001. Interfacial dynamics for Stokes flow. J. Comput. Phys. 169, 250–301.

Prakash, B., Veeregowda, B., Krishnappa, G., 2003. Biofilms: a survival strategy of bacteria. Curr. Sci. India 85, 1299–1307.

Roberts, M.E., Stewart, P.S., 2004. Modeling antibiotic tolerance in biofilms by accounting for nutrient limitation. Antimicrob. Agents Chemother. 48, 48–52.

Sanderson, S.S., Stewart, P.S., 1997. Evidence of bacterial adaption to monochloramine in *Pseudomonas aeruginosa* biofilms and evaluation of biocide action model. Biotechnol. Bioeng. 56, 201–209.

Shaw, T., Winston, M., Rupp, C.J., Klapper, I., Stoodley, P., 2005. Commanality of elastic relaxation times in biofilm. Phys. Rev. Lett. 93(098102), 1–4.

Stewart, P.S., 1996. Theoretical aspects of antibiotic diffusion into microbial biofilms. Antimicrob. Agents Chemother. 40, 2517–2522.

Stewart, P., Rayner, J., Roe, F., Rees, W., 2001. Biofilm penetration and disinfection efficacy of alkaline hypochlorite and chlorosulfamates. J. Appl. Microbiol. 91, 525–532.

Sufya, N., Allison, D., Gilbert, P., 2003. Clonal variation in maximum specific growth rate and susceptibility towards antimicrobials. J. Appl. Microbiol. 95, 1261–1267.

Vetterling, W.T., Teukolsky, S.A., Press, W.H., Flannerly, B., 2002. Numerical Recipes in C: The Art of Scientific Computing. Cambridge University Press, Cambridge.